Tellus (2003), 55A, 317–327
Printed in UK.

TELLUS
ISSN 0280–6495

Radiative and turbulent fluxes in the nocturnal boundary layer

By KYUNG-JA HA[1] and LARRY MAHRT[2]*, [1]*Department of Atmospheric Sciences, Pusan National University, Pusan 609-735, Korea;* [2]*COAS, Oregon State University, Corvallis, OR 97331 USA*

(Manuscript received 31 October 2002; in final form 25 February 2003)

ABSTRACT

This study examines the relative contributions of turbulent and radiative flux divergences to nocturnal cooling by analyzing data from the 60-m flux tower in CASES99 and using an offline model of the radiative flux. The sensitivity of radiative cooling to structure of the atmosphere near the surface is first examined in terms of artificial profiles. In general, the radiative cooling is proportional to the negative curvature of the temperature profile, magnitude of the specific humidity and the deficit of the ground surface temperature. For the days examined, the radiative flux divergence appears to control the initial formation of the surface inversion at the beginning of the night when the turbulence collapses.

1. Introduction

Our understanding of the influence of radiative flux divergence on the nocturnal boundary layer is limited. Garratt and Brost (1981), André and Mahrt (1982), Estournal and Guedalia (1985), Tjemkes and Duynkerke (1989), Duynkerke (1999) and Sun et al. (2003) all found that the radiative flux divergence can contribute significantly to cooling of clear air in the nocturnal boundary layer. Räisänen (1996) showed that the radiative cooling of the air near the surface is sensitive to the details of the temperature profile close to the ground surface, and any discontinuities of temperature at the ground surface. As a result, he found that very high vertical resolution is required to obtain even the correct sign of the radiative flux divergence at the ground surface. Tjemkes and Duynkerke (1989) concluded that the inclusion of radiative flux divergence in a boundary-layer model can reduce the stability of the boundary layer and increase the calculated boundary layer height by about 25%.

Sun et al. (2003) found that the radiative flux divergence controls the formation of the surface inversion in the early evening when the turbulence near the surface collapses. They found that measurements of the radiative flux require careful matching of the surface footprint of the radiometers deployed at different heights even over weak heterogeneity. This was accomplished with a network of downward pointing radiometers at the surface. As in André and Mahrt (1982), they found that between days, the radiative flux divergence varies less than the turbulence flux divergence, so that the importance of clear air radiative cooling is determined mainly by the absence of significant turbulence. Soler et al. (2002) found that radiative flux divergence near the surface caused rapid cooling of the air in the early evening in a small gully.

It is not clear how the omission of clear air radiative cooling in most boundary-layer models affects the adjustment of model parameters (tuning). The adjustment of the turbulent parameterization in Kondo et al. (1978) or restrictions on minimum wind speed or friction velocity are commonly used to provide more downward heat transport in very stable conditions to ameliorate excessive model cooling. Additional causes of excess surface cooling are detailed in Delage et al. (2002). Nocturnal boundary-layer models also do not adequately capture generation of turbulence above the "boundary layer" and downward bursting of turbulence toward the surface, found to be important in the observations of Smedman (1988), Ohya et al.

*Corresponding author.
e-mail: mahrt@coas.oregonstate.edu

(1997), Mahrt (1999) and Mahrt and Vickers (2002). Such turbulence may re-establish the significance of turbulence mixing near the surface and reduce the relative influence of radiative flux divergence. The interaction of turbulence and radiative flux divergences is poorly understood. Since the radiative flux divergence depends on the thermal structure of the nocturnal boundary layer but also modifies the thermal structure, the interaction between the radiative and turbulent flux divergences may be quite complex.

This study examines such interaction using eight levels of eddy correlation data and detailed thermal structure observed in CASES99 (Sun et al., 2002; Burns et al., 2003) and an offline radiation model applied to such thermal structure. As in Maki et al. (1986) and Sun et al. (2003), and perhaps most real nocturnal boundary layers, horizontal advection of temperature plays an important role. The use of the radiation model in the present study allows more detailed vertical structure than in Sun et al. (2003), although the results are only as good as the assumptions of the radiation model.

2. The CASES99 observations

CASES99 was carried out over grassland in south central Kansas, USA during October 1999 (Blumen, 1999; Poulos et al., 2002). The main site includes a 60-m tower system with eight levels of eddy correlation data, 34 levels of thermocouple data from 0.23 to 58.10 m (Sun et al., 2002), R.M. Young propeller anemometer and wind vane data at 15, 25, 35 and 45 m and aspirated thermistor data at 5, 15, 25, 35, 45 and 55 m.

Turbulent fluxes were evaluated using fast response data at six levels (10, 20, 30, 40, 50 and 55 m) of the 60-m tower and two levels (1.5 and 5 m) on a 10-m tower adjacent to the main tower. The data were collected at 20 Hz. The data were quality controlled following Vickers and Mahrt (1997). Fluxes were computed based on perturbations from an averaging window which depends on height and stability (Vickers and Mahrt, 2003). To reduce random flux errors, fluxes are then averaged over 60-min periods.

The eddy diffusivity for level z is computed as

$$K_{\mathrm{mu}} = \frac{u_*^2(z)}{|\mathrm{d}V/\mathrm{d}z|} \tag{1}$$

where the wind shear, $\mathrm{d}V/\mathrm{d}z$, is calculated from the R.M. Young propeller anemometers and wind vane data with finite differencing, and u_*^2 is the magnitude of the momentum flux at level z.

2.1. Four case studies

The nights of 20–21, 21–22, 22–23 and 24–25 October are selected as four contrasting clear sky cases during a period of generally clear skies. All four selected nights experience strong cooling near the surface in the early evening. As the evening proceeds, the cooling rate decreases and vanishes or temporarily reverses to warming on the second, third and fourth nights (Fig. 1, solid lines). The warming events sometimes occur with the onset of turbulent mixing

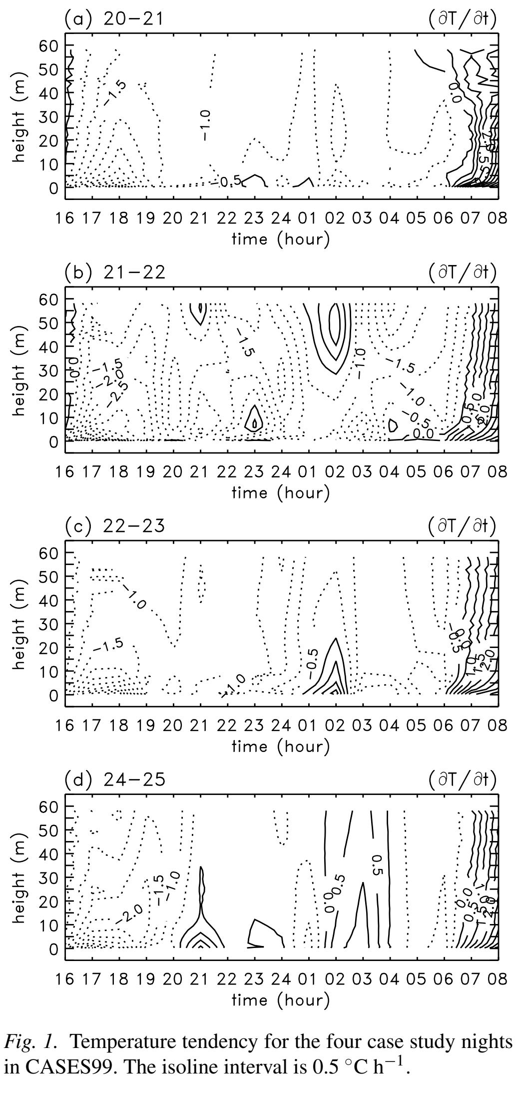

Fig. 1. Temperature tendency for the four case study nights in CASES99. The isoline interval is 0.5 °C h^{-1}.

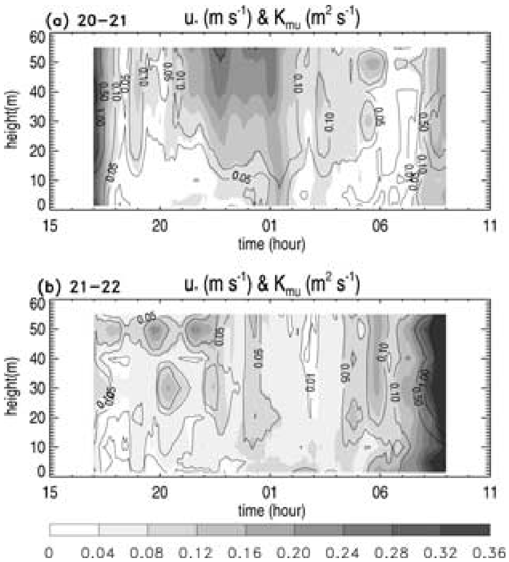

Fig. 2. Time-height sections of the 30-min averaged frictional velocity (shading, bar legend identifies shading scale in m s^{-1}) and eddy diffusivity [eq. (1)] calculated from wind and frictional velocity for the nights of 20–21 and 21–22 October. The intervals for the eddy diffusivity are 0.0005, 0.001, 0.005, 0.01, 0.05, 0.1 and 0.5 $m^2\ s^{-1}$.

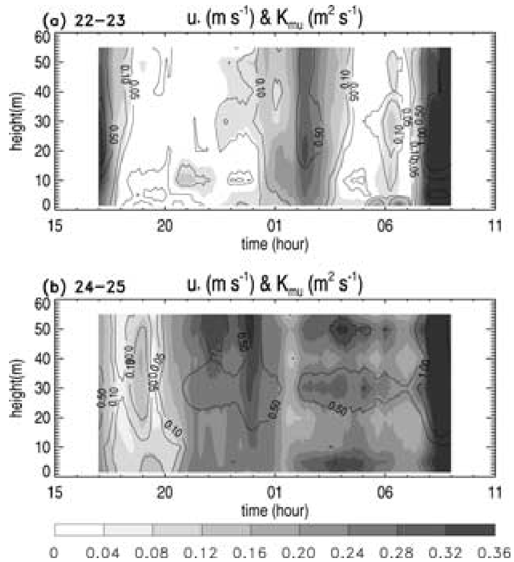

Fig. 3. Same as Fig. 2 but for the nights of 22–23 and 24–25 October.

and downward heat flux, as on the third and fourth nights (Fig. 1). Other warming events are not associated with a turbulence event, as on the second night, and may be due to temperature advection.

The first night (Fig. 2a) includes a major mixing event in the upper part of the tower layer beginning about 2200 LST, the second night includes a few weaker mixing events near the top of the tower (Fig. 2b), the third night includes a major mixing event beginning around 0200 (Fig. 3a), which occupies the entire tower layer, and the fourth night (Fig. 3b) includes a mixing event in the upper part of the tower layer, beginning around 2200, which yields to layering of turbulence after 0200. Such mixing events were common in the middle of the night, with increasing shear associated with nocturnal accelerations and the low-level jet (Mahrt and Vickers, 2002). The layering was not typical. Some nights may be complicated by density currents and propagating disturbances (Sun et al., 2002).

3. Model

We use version 1.0.2 of the CRM (column radiation model) of the Community Climate Model (Kiehl and Briegleb, 1991). Short-wave and long-wave fluxes and the heating rate are computed with a time step of 20 s. The vertical grid spacing is 1 m near the surface and increases at higher levels. Absorption by CO_2, H_2O and O_3, CH_4, N_2O and Chlorofluorohydrocarbons (CFCs) are included. This model adopts the δ–Eddington approximation for shortwave scattering and absorption, with 19 spectral intervals from 0.2 to 5.0 μm radiation. The long-wave radiative transfer is based on an absorptivity and emissivity formulation of Ramanathan and Downey (1986):

$$F\downarrow(p) = B(0)\,\epsilon\,(0, p) + \int_0^p \alpha(p, p')\,\mathrm{d}B(p') \qquad (2)$$

$$F\uparrow(p) = B(T_s) - \int_p^{p_s} \alpha(p, p')\,\mathrm{d}B(p') \qquad (3)$$

where p is pressure, p_s is the surface pressure, $B(T)$ is the blackbody radiation, α is the absorptivity and ϵ is the emissivity. The surface emissivity is assumed to be one. The fluxes at each model level are formulated in terms of the broadband model of Kiehl and Briegleb (1991). The broadband formulation is employed for H_2O, CO_2, CH_4, O_3 and N_2O with minor absorption bands for CO_2. The role of CFCs is approximated with an exponential transmission function. In this study, the mixing ratios of CO_2, N_2O, CH_4, CFC11 and CFC12 are specified as constants equal to 355 ppm, 0.31 ppm, 1.71 ppm, 0.28 ppb and 0.503 ppb, respectively. For the upper atmosphere above the troposphere, we assume radiative equilibrium with the atmospheric temperature profile. For each layer, the clear-air long-wave radiative heating rate is obtained from the net divergence of the spectrally integrated upward ($F\uparrow$) and downward ($F\downarrow$) fluxes.

4. Radiative cooling for idealized vertical structure

4.1. *Temperature and moisture profiles*

Unfortunately, our analysis must be carried out in terms of both temperature, which dictates the radiative flux, and potential temperature, which controls the mixing and is directly predicted in models. The nocturnal boundary layer is often characterized by a decreasing positive temperature gradient with height, corresponding to negative curvature of the temperature profile. In cases with weaker stability and significant wind, the potential temperature may be partially mixed with a capping inversion, in which case the curvature of the temperature profile is positive in the upper part of the boundary layer. Here, we examine the dependence of the radiative flux divergence on the structure of the temperature profile.

The potential temperature profile for the nocturnal surface inversion is often modelled as (see references in Stull, 1988; chap. 12)

$$\theta(z) = \theta_{\mathrm{sfc}} + \Delta\theta[1 - \exp(-z/H)] \tag{4}$$

which corresponds to negative curvature of potential temperature near the surface (Fig. 4), yielding to nearly constant potential temperature at higher levels in an idealized residual layer. Here, H is the scale depth of the inversion layer, $\Delta\theta$ is the strength of the inversion, and the curvature of the potential temperature profile is

$$\frac{\partial^2\theta}{\partial z^2} = \frac{\Delta\theta}{H^2}[1 - \exp(-z/H)]. \tag{5}$$

Potential temperature from this expression is converted to temperature for use in the offline radiation model. For shallow layers, such as the nocturnal boundary layer, the curvature of temperature and potential temperature are approximately equal.

The partially mixed case is crudely represented with an oscillating temperature profile of the form (Fig. 4)

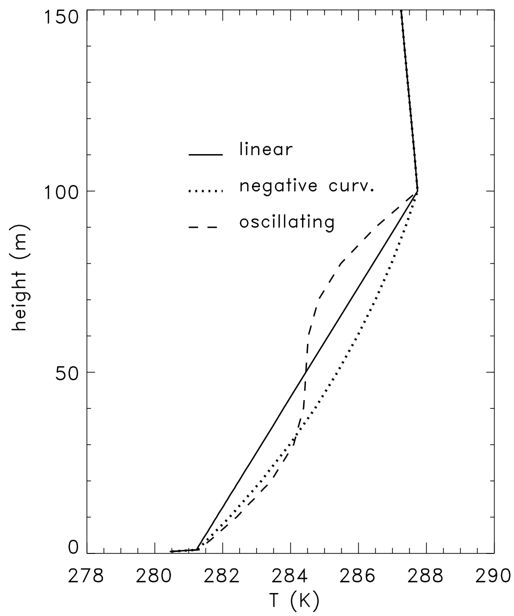

Fig. 4. Idealized temperature profiles for use in the offline model. Above 100 m, potential temperature is constant with height.

$$T(z)_{\mathrm{osc}} = \gamma z + \Delta T \sin\left(\frac{2\pi z}{H}\right) \tag{6}$$

where γ is the rate of increase of temperature with height and H is the vertical wavelength. The curvature of the temperature profile

$$\frac{\partial^2\theta}{\partial z^2} = -4\pi^2\frac{\Delta T}{H^2}\sin\left(\frac{2\pi z}{H}\right) \tag{7}$$

is negative near the surface and positive in the upper part of the boundary layer.

The water vapor mixing ratio is specified to be independent of height with a value of 6.0 g kg^{-1} below 50 m and matched to be height-independent relative humidity above 50 m, approximately 30%. The clear-air effective emissivity produced by the model, which is a function of vapor pressure and temperature, is between 0.7 and 0.8 for these cases in the boundary layer.

4.2. *Vertical structure of radiative cooling*

Stronger radiative cooling occurs with the negatively curved part of the oscillating temperature profile (Fig. 5), while weaker radiative cooling occurs with positive curvature of the temperature profile

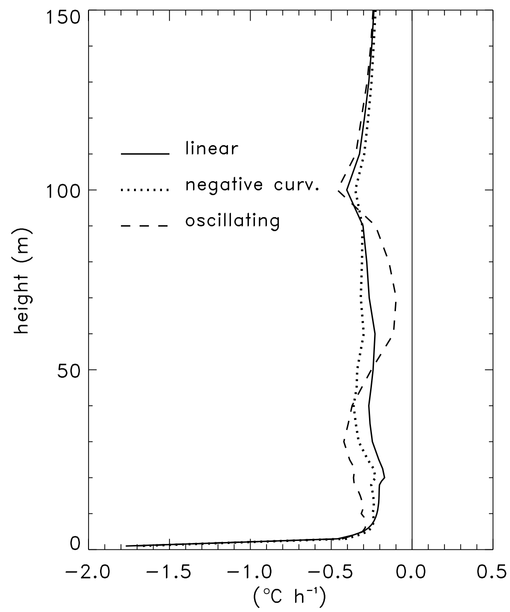

Fig. 5. Radiative cooling rates for the three idealized temperature profiles (Fig. 4).

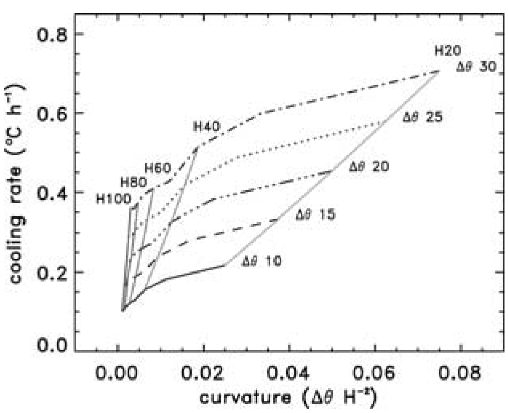

Fig. 6. The cooling rate computed from the offline model as a function of curvature of the negative curved temperature profile. Solid lines correspond to constant depth scale and variable inversion strength while broken lines correspond to constant inversion strength and variable depth scale.

(upper part of the oscillating profile). The profile with negative curvature at all levels has the greatest layer-integrated cooling. The strongest radiational cooling occurs next to the ground surface for all three idealized profiles. The radiative cooling is not uniquely related to the curvature of the temperature profile (Fig. 6).

The structure of the thin layer of strong cooling next to the surface is sensitive to the air–surface temperature difference, and can reverse to weak warming when the ground surface temperature is equal to the air temperature at the lowest model level, as shown in Räisänen (1996). He found that substantially greater radiative cooling of the air occurred with specification of a temperature discontinuity at the ground surface, as compared to the interpolating between 2 m and the surface with a logarithmic profile. The actual atmospheric temperature profile may be somewhere between these two cases, with extremely strong vertical temperature gradients concentrated in the viscous sublayer and decreasing temperature gradient with height in the overlying surface layer. Vegetation complicates this picture in an unknown way.

In Fig. 5 the surface temperature was specified to be 1.5 °C cooler than the theoretical air temperature extrapolated to the surface. This air–surface temperature difference is based on the averaged nocturnal condition for CASES99. If the surface temperature is specified to be equal to the temperature at 1 m, the first model level, the radiative flux divergence switches to warming close to the surface. For the offline model, the radiative cooling near the surface increases approximately linearly with increasing air–surface temperature difference (Fig. 7). These results imply that the surface energy budget exerts a strong influence on the radiative flux divergence in the nocturnal boundary layer.

The radiative cooling is dominated by the divergence of the upward longwave radiation (Fig. 8), as also observed by Sun et al. (2003). The divergence of the downward component leads to weak cooling below 70 m and weak warming above, so that its contribution

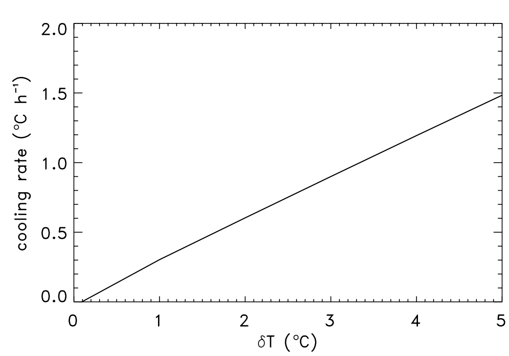

Fig. 7. Radiative cooling rate (°C h^{-1}) for the layer from the surface to 10 m as a function of δT, the air temperature minus the ground temperature.

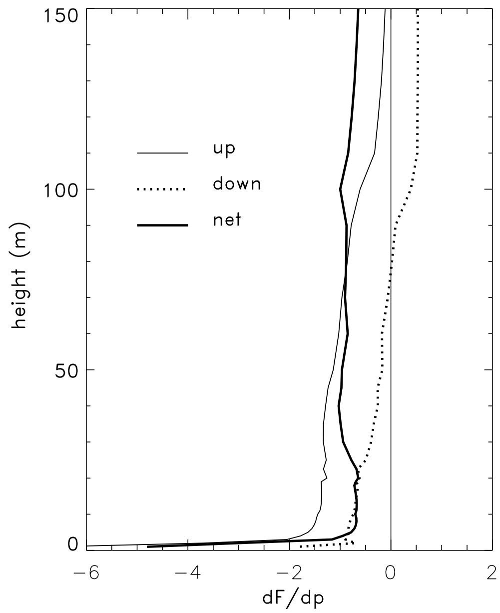

Fig. 8. Radiative flux divergence [W m^{-2}/(kg m^{-1} s^{-2})] due to upward and downward radiative flux for the case of negative curvature of temperature (Fig. 4).

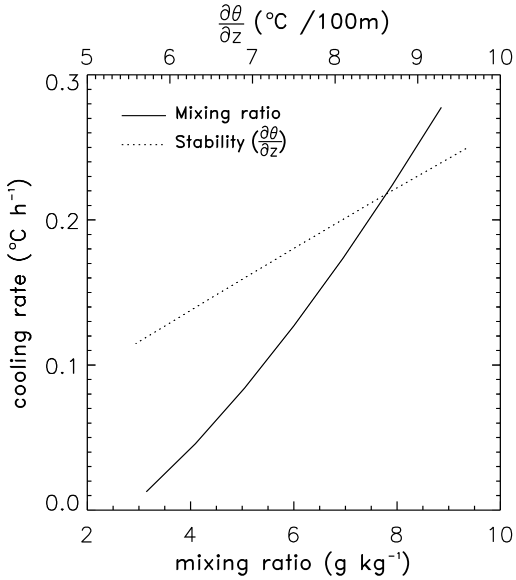

Fig. 9. Modeled radiative cooling rate at the 25-m model level estimated from the offline model as a function of water vapour mixing ratio at that level (solid line) and as a function of stratification for a range of large values observed close to the surface. The temperature profile is linear and the moisture profile is specified as in section 4.2.

is particularly small when integrated over the lowest few hundred metres.

In the early evening, the relative humidity sometimes increases due to decreasing temperature, although increasing water vapor mixing ratio in the early evening sometimes plays a role. The increase of water vapor mixing ratio in the early evening close to the surface is due to continued evaporation at the surface (albeit weak) accompanied by rapidly decreasing strength of the mixing (Acevedo and Fitzjarrald, 2001), although this effect was small for the dry soil conditions in CASES99. To examine the sensitivity of the radiative cooling to the humidity, the water vapor mixing ratio below $H = 50$ m is varied from 3.0 to 9.0 g kg^{-1}, and is again matched to height-independent relative humidity above 50 m. The radiative cooling rate increases monotonically with increasing mixing ratio (Fig. 9, solid line). With greater moisture content, both absorption and emission within the atmosphere increase. For a height-independent mixing ratio and linear temperature profile from 100 m to the ground surface, the radiative cooling also increases systematically with stability (Fig. 9, dotted line).

The radiative flux divergence is only weakly influenced by the observed vertical gradients of moisture in CASES99, which were usually weak. The specific humidity was generally well mixed in the daytime and nocturnal downward moisture flux, and dew formation was normally too limited to generate significant systematic vertical gradients of specific humidity at night. Occasionally, transient disturbances generated significant vertical gradients of moisture, greater than 1.0 g kg^{-1} over the lowest 50 m, which lasted for one or two hours. The lowest level of moisture measurements was 5 m, and vertical moisture gradients below that level would be undetected. Imposing a vertical increase or decrease of 2.0 g kg^{-1} across the lowest 50 m did not substantially change the radiative cooling based on the temperature profiles in Fig. 4. For the observed profiles analyzed in André and Mahrt (1982), the influence of vertical gradients of moisture on the radiative cooling was also secondary.

Although the atmospheric water vapor is the primary absorber and emitter, the radiative flux divergence is determined mainly by the vertical variation of the temperature of the water vapor, rather than the vertical gradient of the water vapor content for the typical vertical moisture gradients in CASES99. In summary,

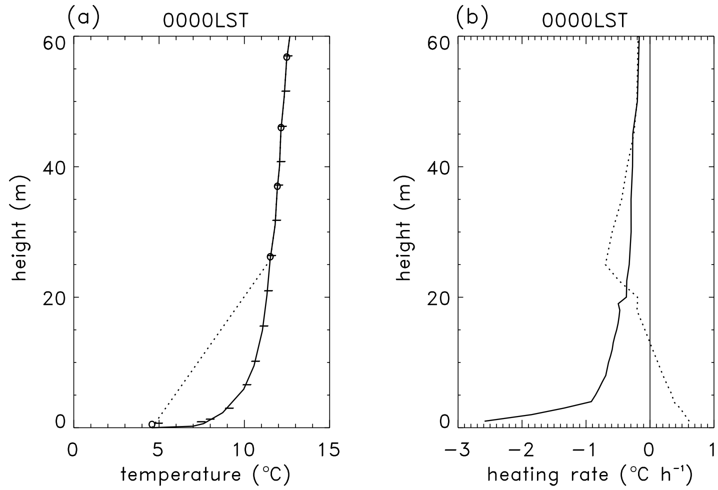

Fig. 10. (a) Temperature profiles for fine vertical resolution (solid line) and poor vertical resolution (dotted line) and (b) corresponding radiative cooling rate predicted by the offline model.

the radiative cooling increases with the stratification, moisture content and negative curvature of the temperature profile.

4.3. Cooling to space

Savijärvi (1990) found that reorganizing the radiative cooling into cooling to space, exchange with the surface and exchange with other levels in the atmosphere [his eq. (9)] facilitates interpretation of the radiative cooling profiles. For the applications examined in Savijärvi (1990), the cooling to space term was the largest term, the cooling to the ground surface was a little smaller, while the exchange with other atmospheric levels was an order of magnitude smaller. For the boundary-layer situations in the present study, the cooling to space term is also the largest term, while the term associated with cooling to the surface is a little smaller. For the negatively curved temperature profile in Fig. 4, the radiative exchange with the other atmospheric levels is 35% of the cooling to space term. However, the curvature in the idealized profiles is generally larger and more organized than in the actual profiles, where the radiative cooling due to the exchange with other levels becomes almost an order of magnitude smaller than the cooling to space term.

4.4. Vertical resolution

Because of the sensitivity of the radiative flux divergence to the temperature profiles close to the surface, poor vertical resolution near the surface can lead to large errors in the longwave radiative flux (e.g., Räisänen, 1996). Here, poor vertical resolution causes erroneous radiative warming near the surface, as is evident from the comparison of two different resolutions of temperature (Fig. 10). The radiation model was run at the same model resolution for each test, but in the simulation of crude vertical resolution of temperature the temperature is linearly interpolated between 25 m and the surface (dotted line on left panel of Fig. 10). At higher levels, the radiative cooling for the case of crude vertical resolution for the temperature input data is similar to that for the case of fine-resolution temperature input data. However, near the surface, the linear interpolated temperature profile leads to radiative warming, while the results with good vertical resolution correspond to substantial cooling, associated with the resolved negative curvature of the temperature profile. As a result, radiative calculations based on coarse observational structure, or based on typical model vertical grid spacing, will provide poor estimates of the clear air radiative cooling near the surface and miss the stabilization of the air near the surface by the radiative flux divergence. As an aside, the small irregularities in the vertical profiles of radiative cooling in Fig. 5 occur at locations where the vertical resolution changes with height.

5. Application to CASES99 observations

We now contrast the vertical structure between the early evening (1800 LST) and the middle of the night

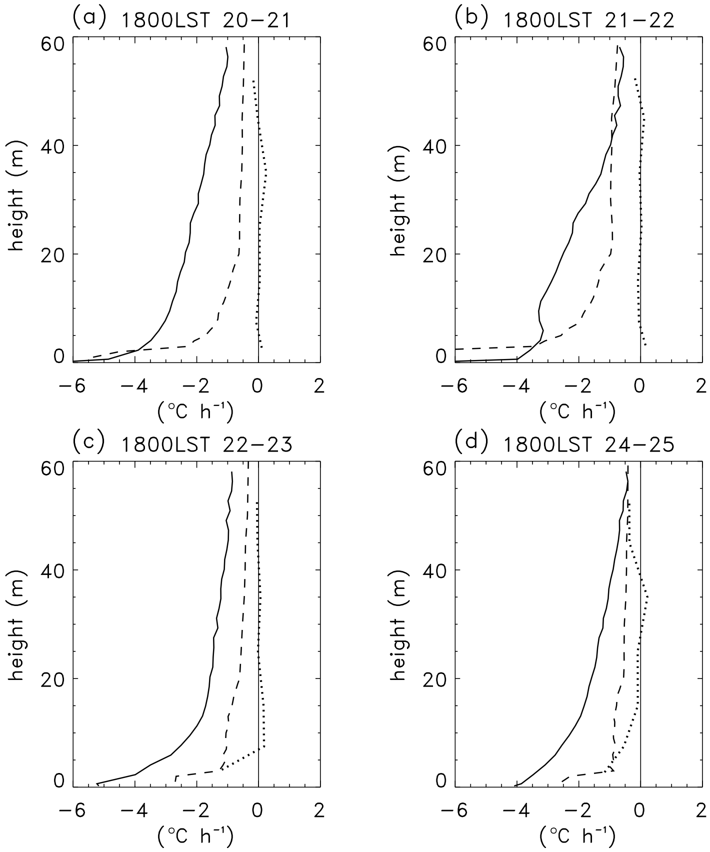

Fig. 11. The vertical profile of the observed cooling (solid line), radiative cooling (dashed line) and the cooling due to turbulent flux divergence (dotted line) for the early evening.

(0000) for the four case study nights (Figs. 11 and 12). Some of the hours are excluded due to flow through the tower. The net local cooling is estimated in terms of the one-hour change of temperature centered on the evaluation time. The calculation of the turbulent flux divergence is detailed in section 2. The radiative cooling rate is computed from the offline radiation model and observed profiles.

The air close to the surface cools rapidly in the early evening due primarily to radiative flux divergence (dashed line, Fig. 11), as also observed in Sun et al. (2003). On the first case study night, the observed and radiative cooling rates both reach 6.0 °C h^{-1} close to the ground surface. The radiative cooling decreases with height and therefore acts to stabilize the air near the surface. It appears that the formation of the surface inversion is dominated by radiative flux divergence and that the turbulent heat flux plays a secondary role, assuming that the turbulent heat fluxes are adequately estimated.

As the evening proceeds, the flow accelerates and increasing shear generate turbulence (Mahrt and Vickers, 2002). By the middle of the night, the turbulence heat flux divergence may be of either sign, causing warming or cooling. For the four cases study nights at 0000 LST, significant cooling due to the turbulent heat flux divergence is confined to the lowest 20 or 30 m for the first two cases (Fig. 12), while it is poorly defined for the other two cases. The erratic behavior of the turbulent cooling can be identified with the event-like behavior of the mixing (Figs. 2 and 3). For the middle of the night, the calculation of the radiative cooling profile was extended well above the tower using slow-ascent radiosonde temperature data in the

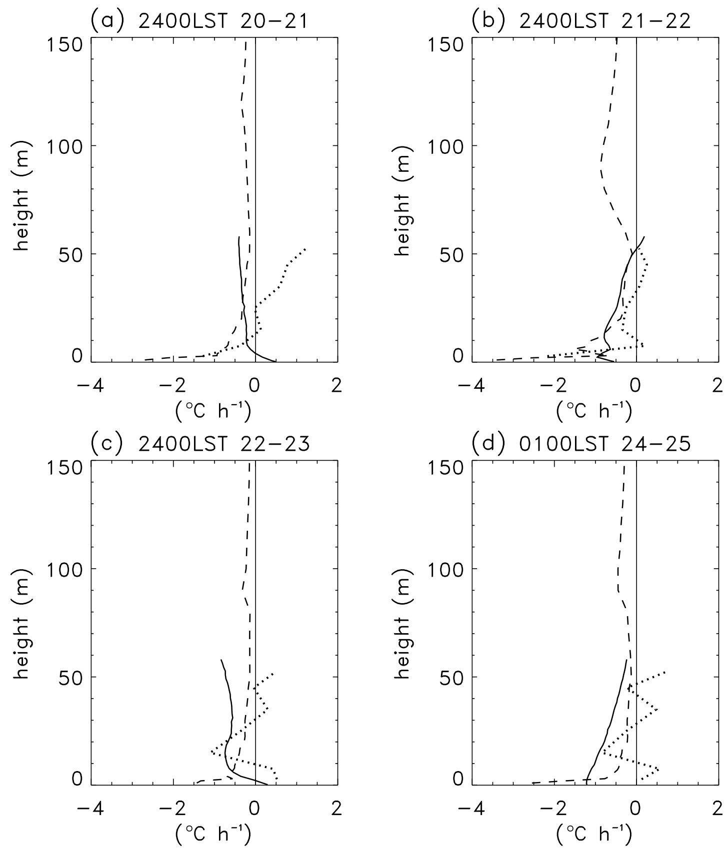

Fig. 12. The vertical profile of the observed cooling (solid line), radiative cooling (dashed line) and the cooling due to turbulent flux divergence (dotted line) for the middle of the night.

offline model. The most significant radiative cooling is again confined to a very thin layer near the surface.

Since the observed cooling is not generally balanced by the radiative and turbulent flux divergences, significant errors or an additional source of cooling are implied, such as cold air advection. Solving for the horizontal temperature advection from the thermodynamic equation

$$\boldsymbol{V} \cdot \nabla\overline{\theta} = -\frac{\partial\bar{\theta}}{\partial \boldsymbol{t}} - \frac{\partial\overline{\theta'\boldsymbol{w}'}}{\partial \boldsymbol{z}} - \frac{1}{\rho \boldsymbol{C_p}}\frac{\partial \boldsymbol{F_n}}{\partial \boldsymbol{z}} \tag{8}$$

where the overbar denotes a time average, $\boldsymbol{V}$ is the wind vector, the first term on the right-hand side is the mean temperature tendency (net local cooling), the second term is the turbulent heat flux divergence, and the third term is the radiative flux divergence. The temperature advection is computed as a residual, which is likely strongly influenced by errors in the terms on the right-hand side. Positive values of $\boldsymbol{V} \cdot \nabla\theta$ correspond to cold air advection.

The residual of the thermodynamic equation for 20–21 October is positive next to the surface (Fig. 13), possibly implying significant cold air advection near the surface, which could be due to advection by the southerly flow of colder air over lower terrain which slopes downward south of the tower for 1.5 km (Mahrt et al., 2001). The large residual could also be due to underestimation of turbulent and radiative flux divergences. Note that the residual would be even greater if the radiative flux divergence were omitted. Above 10 m, the residual is negative, possibly implying warming due to subsidence.

A relatively small horizontal temperature difference could account for the unexplained cooling. As an example, for an unexplained cooling rate of 1 °C h^{-1}, the required temperature difference between the tower

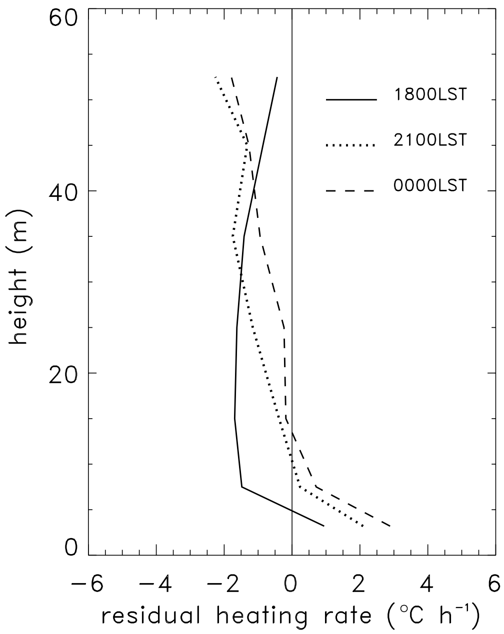

Fig. 13. The residual heating rate for three different periods on 20–21 October. Positive values could be explained by cold air advection.

and lower terrain 1 km upstream is

$$\Delta\theta = \frac{10^3\mathrm{m}}{v}\frac{1\,^\circ\mathrm{C}}{3.6 \times 10^3\mathrm{s}}. \tag{9}$$

For a wind speed of 3 m s^{-1}, this corresponds to a potential temperature difference of only about 0.1 °C! The observed horizontal difference of the temperature is much larger, although the coldest air is in small gullies (Mahrt et al., 2001), and it is difficult to determine a representative upstream temperature. Nonetheless, even choosing the warmest possible value for the upstream potential temperature, the cold air advection is comparable to, or larger, than that required to balance eq. (9). That is, for stable nocturnal conditions, local temperature advection can be large even for this site, where slopes are only a few percent or less. Over a larger area, one expects regions of both microscale warm air and cold air advection.

6. Conclusions

An offline radiation model applied to artificial profiles of temperature and moisture and profiles from CASES99 data indicate that the radiative cooling increases with the thermal stratification, moisture content, negative curvature of the temperature profile and temperature deficit of the ground surface. For the four case study days in CASES99 with sufficient data, the clear-air radiative flux divergence is the primary contributor to the initial formation of the nocturnal surface inversion, although microscale cold air advection due to gentle topography appears to play an important role. These findings are in agreement with Sun et al. (2003). As the evening proceeds, the flow accelerates and significant turbulence is sometimes generated near the surface, or is exported downward from higher levels, and the turbulent flux divergence term usually becomes significantly larger than the radiative fluxdivergence term. The estimated radiative and turbulent flux divergences are, on average, not large enough to balance the observed cooling.

7. Acknowledgments

The extensive comments of P. Räisänen and discussions with James Coakley and Jielun Sun are greatly appreciated. Important comments on the final manuscript by Branko Grisogono and one of the reviewers are also gratefully acknowledged. This material is based upon work supported by R05-2001-00262 from the Korean Science and Engineering Foundation and Grant DAAD19-02-1-0224 from the Army Research Office and Grant 0107617-ATM from the Physical Meteorology Program of the National Sciences Foundation.

REFERENCES

Acevedo, O. C. and Fitzjarrald, D. R. 2001. The early evening surface-layer transition: Temporal and spatial variability. *J. Atmos. Sci.* **58**, 2650–2667.

André, J.-C. and Mahrt, L. 1982. The nocturnal surface inversion and influence of clear-air radiative cooling. *J. Atmos. Sci.* **39**, 864–878.

Blumen, W. 1999. CASES99 Field Catalog, *http://www.joss.ucar.edu/cases99/catalog*.

Burns, S., Sun, J., Delay, A. C., Horst, T. W. and Oncley, S. P. 2003. A field intercomparison technique to improve the relative accuracy of longwave radiation measurements and an evaluation of CASES-99 pyrgeometer data quality. *J. Atm. Ocean. Technol.* **20**, 348–361.

Delage, Y., Bartlett, P. A. and McCaughey, J. H. 2002. Study of “soft” night-time surface-layer decoupling over forest canopies in a land surface model. *Boundary-Layer Meteorol.* **103**, 253–276.

Duynkerke, P. 1999. Turbulence, radiation and fog in Dutch stable boundary layer. *Boundary-Layer Meteorol.* **90**, 447–477.

Estournel, C. and Guedalia, D. 1985. Influence of geostrophic wind on atmospheric nocturnal cooling. *J. Atmos. Sci.* **42**, 2695–2698.

Garratt, J. R. and Brost, R. A. 1981. Radiative cooling effects within and above the nocturnal boundary layer. *J. Atmos. Sci.* **38**, 2730–2746.

Kiehl, J. T. and Briegleb, B. P. 1991. A new parameterization of the absorptance due to the 15 μm band system of carbon dioxide. *J. Geophys. Res.* **96**, 9013–9019.

Kondo, J., Kanechika, O. and Yasuda, N. 1978. Heat and momentum transfers under strong stability in the atmospheric surface layer. *J. Atmos. Sci.* **35**, 1012–1021.

Mahrt, L. 1999. Stratified atmospheric boundary layers. *Boundary-Layer Meteorol.* **90**, 375–396.

Mahrt, L., Vickers, D., Nakamura, R., Sun, J., Burns, S., Lenschow, D. and Soler, M. 2001. Shallow drainage and gully flows. *Boundary-Layer Meteorol.* **101**, 243–260.

Mahrt, L. and Vickers, D. 2002. Contrasting vertical structures of nocturnal boundary layers. *Boundary-Layer Meteorol.* **105**, 351–363.

Maki, M., Harimaya, T. and Kikuchi, K. 1986. Heat budget studies on nocturnal cooling in a basin. *J. Meteorol. Soc. Jpn.* **64**, 727–741.

Ohya, Y., Neff, D. E. and Meroney, R. N. 1997. Turbulence structure in a stratified boundary layer under stable conditions. *Boundary-Layer Meteorol.* **83**, 139–161.

Poulos, G. S., Blumen, W., Fritts, D., Lundquist, J., Sun, J., Burns, S., Nappo, C., Banta, R., Newsome, R., Cuxart, J., Terradellas, E., Balsley, B. and Jensen, M. 2002. CAESE-99: A comprehensive investigation of the stable nocturnal boundary layer. *Bull. Am. Meteorol. Soc.* **83**, 555–581.

Ramanathan, V. and Downey, P. 1986. A nonisothermal emissivity and absorptivity formulation for water vapor. *J. Geophys. Res.* **91**, 8649–8666.

Räisänen, P. 1996. The effect of vertical resolution on clear-sky radiation calculations: tests with two schemes. *Tellus* **48**, 403–423.

Savijärvi, H. 1990. Fast radiation parameterization schemes for mesoscale and short-range forecast models. *J. Appl. Meteorol.* **20**, 437–447.

Smedman, A. S. 1988. Observation of a multi-level turbulence structure in a very stable atmospheric boundary layer. *Boundary-Layer Meteorol.* **44**, 231–253.

Soler, M. R., Infante, C., Buenestado, P. and Mahrt L. 2002. Observations of Nocturnal Drainage Flow. *Boundary-Layer Meteorol.* **105**, 253–273.

Stull, R. B. 1988. *An introduction to boundary layer meteorology.* Kluwer Academic Publishers, Boston, 666 pp.

Sun, J., Burns, S., Delany, A., Horst, T., Oncley, S. and Lenschow, D. 2003. Heat balance in nocturnal boundary layers. *J. Appl. Meteorol.,* in press.

Sun, J., Burns, S., Lenschow, D., Banta, R., Newsom, R., Coulter, R., Frasier, S., Ince, T., Nappo, C., Cuxart, J., Blumen, W., Lee, X. and Hu, X.-Z. 2002. Intermittent Turbulence Associated with a density current passage in the stable boundary layer. *Boundary-Layer Meteorol.* **105**, 199–219.

Tjemkes, S. and Duynkerke, P. 1989. The nocturnal boundary layer: Model calculations compared with observation. *J. Appl. Meteorol.* **28**, 161–175.

Vickers, D. and Mahrt, L. 1997. Quality control and flux sampling problems for tower and aircraft data. *J. Atm. Ocean. Technol.* **14**, 512–526.

Vickers, D. and Mahrt, L. 2003. The cospectral gap and turbulent flux calculations *J. Atm. Ocean. Technol.* **20**, 660–670.